91602
new 82-10

LEGAL NOTICE

This report was prepared by Ontario Hydro and, while effort has been made to assure the accuracy and applicability of the material contained herein, neither Ontario Hydro nor any person acting on its behalf:

(a) makes any warranty, express or implied with respect to the use of any information, apparatus, method or process disclosed in this report or that such use may not infringe privately owned rights; or

(b) assumes any liabilities with respect to the use of, or for damages resulting from the use of, any information, apparatus, method or process disclosed in this report.

ontario hydro
research division

COMPLIMENTARY COPY
Please Credit Ontario Hydro Research if Reproduced in Whole or in Part

THE DISTRIBUTION OF CARBON-14 IN THE OXIDE LAYER ON THE OUTER SURFACE OF AN IRRADIATED ZR-2.5WT% NB PRESSURE TUBE FROM PICKERING UNIT 3

Report No 89-176-K

F.R. Greening
Chemist
Process Chemistry Section
Chemical Research Dept

ABSTRACT

The OD oxide on an irradiated Zr-2.5 wt% Nb pressure tube sample (P3L09) has been investigated by Auger electron, x-ray photoelectron, secondary-ion mass spectrometric, x-ray diffraction and radiometric techniques. The oxide scale was found to be $1.4 \pm 0.2\mu m$ thick with carbon-14 enriched in the topmost 50nm to an average concentration of 8 atom % equivalent to 4 $\mu Ci/cm^2$. Below this surface layer the carbon-14 concentration falls rapidly to the base metal level of about 1×10^{-3} atom %. Nitrogen, possibly as a nitride, was also found to be enriched in the near-surface oxide but at a concentration (~2.5 atom %) insufficient to account for the observed level of carbon-14. It is concluded that the carbon-14 has been deposited from the annulus gas system probably by an ion-implantation mechanism. Limited results for some other isotopes observed in the oxide scale such as ^{1}H, ^{2}D, ^{3}H, ^{11}B, ^{12}C and ^{13}C are also presented and discussed.

job	file	date	report no.
31-572-810	833.74	August 18, 1989	89-176-K

89-06327/

ontario hydro
research division

To: Dr. D.Mills
Director of Research

THE DISTRIBUTION OF CARBON-14 IN THE OXIDE LAYER ON THE OUTER SURFACE OF AN IRRADIATED ZR-2.5WT% NB PRESSURE TUBE FROM PICKERING UNIT 3

1.0 INTRODUCTION

In July of 1987 pressure tube L09 was removed from Pickering Unit 3 after more than 4000 effective full-power days (EFPD) of reactor operation. After removal, this pressure tube was sent to Chalk River Nuclear Laboratories (CRNL) for inspection and analysis. The main thrust of investigations at CRNL has been towards a determination of the distribution of deuterium along the length of the pressure tube. Recently Ontario Hydro Metallurgical Research has used Secondary Ion Mass Spectrometry (SIMS) to depth-profile the deuterium from both the OD and ID surfaces of the tube/1/.

The availability of samples of the L09 tube has prompted the undertaking of additional investigations into a number of other important features of irradiated pressure tubes exposed to a nitrogen-filled gas annulus. In particular studies at Ontario Hydro Chemical Research have been directed towards answering the long-standing question of how much carbon-14 resides on the surface of an irradiated tube. This question was first raised at the time of the retubing of Pickering Units 1 and 2,/2/, and remains an issue for the long term disposal of retubing waste.

In April 1988 oxygen additions to the P3 nitrogen annulus gas were initiated with the intention of oxidizing deposited carbon-14 to $^{14}CO_2$. Measured oxidation rates, based on $^{14}CO_2$ production, have fallen well short of expectations again posing the question of the distribution of carbon-14 within the reactor core.

This report presents the results of studies of the outer diameter (OD) oxide on a sample of the P3L09 pressure tube with particular emphasis on the distribution of carbon-14 in the near-surface layer.

1.1 Experimental Procedures

The sample of irradiated pressure tube used in this investigation consisted of a section, 0.25 cm^2 in area and 0.13 cm thick, cut so that the black outer surface oxide remained undisturbed on the base Zr-2.5%Nb metal. The sample was originally taken 50cm from the inlet end of channel L09 of the Pickering Unit 3 (P3) reactor. A non-irradiated sample of Zr-2.5%Nb taken from a P3 pressure tube off-cut (part #238) was also investigated for comparative purposes.

The irradiated sample was analyzed by an Ortec 7050 gamma-spectrometry system for the determination of gamma-active radionuclides. X-ray emission from the sample was also investigated with a KEVEX 0700 energy dispersive spectrometer.

Crystalline phase identification on the OD surfaces of the irradiated and non-irradiated samples was carried out with a Phillips x-ray diffractometer using Cu Kα radiation. A JAMP-10 scanning Auger microprobe at Chemical Research was also used to analyze the surface of these samples and elemental depth-profiles were acquired with sputtering provided by a 3M minibeam II ion gun.

X-ray photoelectron spectometry (XPS) and secondary ion mass-spectrometry (SIMS) of the samples were undertaken at Surface Science Western using a SSL SSX-100 photoelectron spectrometer and a Cameca IMS 3*f* ion-microprobe.

After the above analyses had been completed the total carbon-14 and tritium content of the irradiated sample was determined. To this end the sample was heated in a tube furnace to 1100°C in a stream of air for twenty hours. The off-gas was drawn through two bubblers connected in series; the first contained 20 mL of 0.01 M H_2SO_4 for the collection of ^3H_2O and the second contained 20 mL of 0.1M NaOH for the collection of $^{14}CO_2$. The total tritium and carbon-14 trapped in the bubblers was measured with a Packard liquid scintillation counter.

2.0 EXPERIMENTAL RESULTS

2.1 Gamma-Spectrometric Analysis

The results of the gamma-spectrometric analysis of the as-received irradiated P3L09 sample are given in Table 2.1.1. Activities are expressed as μCi/sample. (Specific activities in μCi/g may be obtained by dividing the data by the sample weight, 0.216g).

Table 2.1.1.
The Activities of the Gamma-Active
Radionuclides Identified in the
P3L09 Pressure Tube Sample

Radionuclide	Time of Count (15-Mar-89) Activity (μCi)
Mn-54	0.9 ± 0.3
Co-60	18.4 ± 0.8
Zr-95	26.8 ± 0.9
Nb-94	26.0 ± 0.6
Nb-95	54.8 ± 0.9

The most significant result in Table 2.1.1. is the relatively high activity observed for the very long lived isotope Nb-94. In view of the much shorter half lives of the other isotopes in Table 2.1.1. Nb-94 will become the major gamma activity in this sample within two years of removal from the reactor.

A calculation of the neutron activation of a 0.216 g sample of Zr-2.5% Nb exposed to a thermal neutron flux of 5.7×10^{13} n/cm^2/s,/3/, for 4240 EFPD results in a Nb-94 activity of 24 ± 3 μCi, assuming a cross-section of 1.1 ± 0.1 b, in good agreement with the value reported in Table 2.1.1.

Energy dispersive x-ray analysis of the sample of irradiated P3L09 tubing detected emission of Mn x-rays at 5.9 keV in addition to the expected Zr and Nb K x-ray emissions between 15 and 19 keV. The Mn x-rays are characteristic of Fe-55 but no attempt was made to quantify this radionuclide.

In order to determine if any loose radioactive particulate material was present on the surface of the irradiated P3L09 sample it was placed in 5 mL of deionized water and ultrasonically shaken for ten minutes. The resulting solution, containing suspended particulate together with any leached activity, was analyzed by gamma spectrometry and liquid scintillation counting. The gamma-active radionuclides detected in the solution are reported in Table 2.1.2. (The activities in Table 2.1.2 are reported in nCi not μCi.)

Table 2.1.2.
The Activities of Gamma-Active Radionuclides
Ultrasonically Removed from the P309 Sample

Radionuclide	Time of Count (16-Mar-89) Activity (nCi)
Mn-54	0.010 ± 0.003
Co-60	0.163 ± 0.006
Zr-95	0.030 ± 0.004
Nb-95	0.062 ± 0.005
Ru-106	0.201 ± 0.026
Cs-134	0.124 ± 0.005
Cs-137	0.527 ± 0.010
Ce-144	0.324 ± 0.012

Liquid scintillation counting of the ultrasonic test solution showed the presence of about 25 nCi of carbon-14 after correction for the presence of the above gamma-emitters. This is equivalent to 100 nCi/cm^2 of loose carbon-14 on the pressure tube OD surface.

2.2 X-ray Diffraction Analysis

X-ray diffractograms of the outer oxide surfaces of the irradiated P3L09 sample and the non-irradiated off-cut exhibited intense reflections from the zirconium base metal. For the non-irradiated sample the most intense peak was the 2.46 Å (101) reflection in agreement with the JCPDS data for α-zirconium/4/. However, in the irradiated P3L09 sample diffractogram the (101) peak was almost completely suppressed and the 1.62 Å (110) and 1.37 Å (112) reflections showed the highest intensities. This behaviour is indicative of the preferred orientation of some crystallographic planes in the irradiated sample.

The irradiated and non-irradiated sample diffractograms also exhibited weak relections, typically <20% of the major α-zirconium peaks, attributable to non-metallic phases. Thus the peak at 3.16 Å observed with approximately the same intensity in both diffractograms is undoubtedly the (111) reflection of Baddeleyite, ZrO_2.

The irradiated P3L09 sample gave a number of significant reflections which were of very low intensity, or were simply not present, in the non-irradiated sample diffractogram; Table 2.2.1. lists these reflections together with their relative intensities. Table 2.2.2. presents JCPDS data for crystalline phases of zirconium compounds with d-spacings which fit the unidentified peaks in P3L09./4/.

Table 2.2.1 X-Ray Diffractogram Peaks Enhanced in the P3L09 Irradiated Pressure Tube Sample

d-spacing (Å)	Relative Intensity I/I_1
2.63	100
2.51	30
2.31	10
1.64	40
1.49	20
1.38	30
1.32	40
1.13	20

Table 2.2.2 JCPDS Data for Crystalline Phases of Zirconium Compounds Fitting the Unidentified Peaks in the P3L09 Diffractogram

ZrN		ZrO	
d-spacing (Å)	Relative Intensity I/I_1	d-spacing (Å)	Relative Intensity I/I_1
2.64	100	2.67	100
2.29	100	2.31	100
1.62	80	1.63	55
1.38	70	1.39	35
1.32	40	1.33	16
1.14	20	1.16	8

It may be seen by comparing Table 2.2.1. with Table 2.2.2 that the d-spacings for six of the reflections observed for the irradiated P3L09 sample coincide very closely with those reported for cubic zirconium nitride, ZrN, although the fit to ZrO is also quite good. Unfortunately the observed intensity ratios for the P3L09 sample are not in agreement with those reported for either ZrN or ZrO. This is not too significant, however, because preferred orientation effects have already been noted for this sample and are generally observed for surface scales measured in-situ.

In summary it is clear that a phase additional to ZrO_2 forms on the surface of Zr-2.5% Nb irradiated in nitrogen, but it remains somewhat uncertain that this phase is ZrN.

2.3 Auger Electron Analysis

Auger electron analysis of the irradiated P3L09 pressure tube sample showed zirconium (~20 at %), oxygen (~55 at %), carbon (~20 at %) and nitrogen (~2 at %) at randomly selected locations on the as-received OD surface. Depth-profiles of these elements were recorded using a 3 keV argon-ion beam operated at a current of 0.5 μA and rastered over an area of about 200 x 200 μm^2. The sputtering rate was estimated from previous measurements to be 8nm/min. Typical depth-profiling data are given in Table 2.3.1

The data in Table 2.3.1 show that the irradiated P3L09 pressure tube oxide scale extends approximately 1.5 μm below the OD surface. The outermost 0.5 μm layer of this oxide contains significant levels of carbon and nitrogen.

Equivalent depth-profiles were recorded for the non-irradiated P3 off-cut using identical sputtering conditions. The oxide-metal interface was found at a depth of approximately 0.8 μm. The outermost 0.2 μm layer of the oxide contained about twice the concentration of carbon as the irradiated sample but less (~ 1 at %) nitrogen.

Table 2.3.1
An Auger Depth-Profile of the P3L09
Irradiated Pressure Tube Sample

Element (At%)	Sputtered Depth (nm)													
	8	20	40	120	240	480	720	960	1200	1440	1680	1920	2160	2400
Carbon	13.9	9.1	6.8	1.9	0.9	0.0	0.0	0.0	0.0	0.0	1.1	1.2	0.7	0.5
Nitrogen	2.4	2.6	2.3	1.7	1.0	0.0	0.0	0.0	0.0	0.0	0.0	0.0	0.0	0.0
Oxygen	57.7	61.8	59.5	61.5	62.2	62.9	63.1	63.4	63.3	64.7	33.9	17.5	3.1	0.9
Zirconium	26.0	26.5	31.4	34.9	35.9	37.1	36.9	36.6	36.7	35.3	65.0	81.3	96.2	98.6

2.4 X-ray Photoelectron Analysis

X-ray photoelectron spectrometry of the irradiated P3L09 pressure tube sample detected zirconium, oxygen, carbon and nitrogen as well as traces of metallic impurities such as iron, copper, tin and lead on the OD surface of the as-received sample. After argon-ion sputtering to a depth of about 200nm and re-analysis of the sputtered surface only zirconium, oxygen and carbon could be detected. Table 2.4.1 records the abundances of these elements measured before and after sputtering.

Table 2.4.1
X-Ray Photoelectron Analysis of the Irradiated
P3L09 Sample Before and After Sputtering

Element (At%)	As - Received Surface	Sputered to 200 nm
Carbon	48.6	6.8
Nitrogen	2.3	0.0
Oxygen	37.9	48.7
Zirconium	11.2	44.5

High-resolution scans of the zirconium, oxygen, carbon and nitrogen photoelectron spectrum peaks were also carried out for the as-received irradiated P3L09 sample. Unfortunately specimen charging induced distortion of the low binding-energy side of the peaks ruling out reliable chemical state analysis especially for the low abundance peaks. In the case of the high abundance carbon 1s peak the binding energy of the peak maximum was certainly indicative of mainly organic carbon.

A spectrum of the P3 off-cut was also acquired for comparative purposes. Zirconium, oxygen and carbon, but no nitrogen, were detected on the as-received surface.

2.5 Secondary-Ion Mass Spectrometric Analysis

Secondary-ion Mass Spectrometry (SIMS) was carried out using a Cs^+ primary beam current between 100nA and 800nA and an accelerating voltage of 10kV. The beam was rastered over 250 μm. Negative secondary ions were mass analyzed with a 100V off-set to minimize interferences from molecular species.

The principal mass-spectral peaks observed for the irradiated P3L09 sample compared to the non-irradiated P3 off-cut are reported in Table 2.5.1. The parent ion assignments in this table have been made on the basis of the following considerations:

(i) Other surface analysis techniques used in the present investigation have shown zirconium, oxygen, carbon and nitrogen to be the major elements present on the surface of the samples.

(ii) The negative-ion yield of carbon is very high. By comparison the yield of nitrogen is so low that it is considered to be non-detectable by Cs^+ bombardment/5/

(iii) For the non-irradiated sample natural isotopic abundances should be observed.

(iv) The relative intensities observed for m/e=12, 13 and 14 in the non-irradiated sample show that ^{12}CD and $^{12}C^1H_2$ contribute no more than 1% to the observed intensity of the m/e=14 peak in the irradiated sample. Thus the identification of ^{14}C may be arrived at by a process of elimination.

(v) The parent-ion assignments of all other mass peaks are made with the proviso that molecular ions such as MO, MH or MD are allowed to contribute up to 100% of the intensity observed for the atomic, M, peak.

It is instructive to examine the data in Table 2.5.1 by comparing the intensities observed for the irradiated sample with those for the non-irradiated sample. The most significant feature of the data analysed on this basis is the occurrence of significant intensities of the species D, ^{11}B and ^{14}C in the irradiated sample. It is evident that ^{11}B originates in a nuclear process in view of the virtual absence of ^{10}B. It will be shown in an appendix to this report that ^{11}B is probably produced by a (n,α) reaction on ^{14}N.

Depth-profiles of D and ^{14}C were acquired for the irradiated P3L09 sample by long-term sputtering with a 65nA Cs^+ beam with monitoring of the m/e=2 and m/e=14 secondary-ions; m/e = 1 and 12 were also monitored for comparative purposes. In addition, to determine the location of the oxide/base metal interface the m/e=90 and m/e=106 intensities were also simultaneously monitored.

Table 2.5.1 SIMS Negative-Ion Intensity Data for the P3L09 (Irradiated) and P3 Off-Cut (Non-Irradiated) Samples

m/e	Peak Intensity (counts/s)		Parent Ions
	P3 Off-Cut (Non-Irradiated)	P3L09 (Irradiated)	
1	2.06×10^4	1.89×10^4	^{1}H
2	-	3.40×10^4	^{2}H (D)
10	1.0×10^1	4.0×10^0	^{10}B
11	2.30×10^1	3.48×10^3	^{11}B
12	1.16×10^5	3.49×10^4	^{12}C
13	1.52×10^3	9.38×10^2	^{13}C, $^{12}C^{1}H$
14	1.30×10^1	1.40×10^5	^{14}C, ^{12}CD, $^{12}C^{1}H_2$
16	3.08×10^6	2.96×10^6	^{16}O
17	1.28×10^5	6.65×10^4	^{17}O, $^{16}O^{1}H$
18	2.46×10^5	2.90×10^5	^{18}O, ^{16}OD
19	1.33×10^4	2.28×10^4	^{19}F, $^{18}O^{1}H$
28	3.93×10^3	1.26×10^4	^{28}Si, $^{14}C_2$, $^{14}C^{14}N$
32	2.51×10^5	1.53×10^5	$^{16}O_2$
56	5.75×10^2	1.72×10^3	^{56}Fe
72	1.48×10^2	1.68×10^3	$^{56}Fe^{16}O$
90	2.20×10^4	7.43×10^4	^{90}Zr
91	7.82×10^3	1.67×10^4	^{91}Zr, $^{90}Zr^{1}H$
92	7.86×10^3	3.54×10^4	^{92}Zr, $^{91}Zr^{1}H$, ^{90}ZrD
93	4.81×10^3	1.06×10^4	^{93}Nb, $^{92}Zr^{1}H$, ^{91}ZrD
94	6.80×10^3	3.00×10^4	^{94}Zr, ^{92}ZrD
95	1.07×10^3	1.29×10^3	^{94}ZrH
96	1.07×10^3	7.16×10^3	^{96}Zr, ^{94}ZrD
106	2.10×10^4	3.75×10^5	$^{90}Zr^{16}O$
107	3.36×10^3	8.82×10^4	$^{91}Zr^{16}O$
108	5.87×10^3	1.37×10^5	$^{92}Zr^{16}O$
109	5.12×10^2	9.32×10^3	$^{93}Nb^{16}O$
110	5.01×10^3	1.22×10^5	$^{94}Zr^{16}O$
112	7.37×10^2	1.89×10^4	$^{96}Zr^{16}O$

Table 2.5.2 The Intensities of Ions Monitored During the Sputter-Profiling of the P3L09 Irradiated Pressure Tube Sample

m/e	Sputtered Depth (nm)																	
counts/s	10	20	40	60	80	100	125	150	175	200	250	300	400	500	600	800	1000	1200	1400
1	1.82 $\times 10^{4}$	2.16 $\times 10^{4}$	1.42 $\times 10^{4}$	9.84 $\times 10^{3}$	8.77 $\times 10^{3}$	8.01 $\times 10^{3}$	7.41 $\times 10^{3}$	6.95 $\times 10^{3}$	5.99 $\times 10^{3}$	5.41 $\times 10^{3}$	4.91 $\times 10^{3}$	4.09 $\times 10^{3}$	3.97 $\times 10^{3}$	4.03 $\times 10^{3}$	6.29 $\times 10^{3}$	1.58 $\times 10^{4}$	1.69 $\times 10^{4}$	4.61 $\times 10^{3}$	3.05 $\times 10^{3}$
2	1.66 $\times 10^{5}$	1.61 $\times 10^{5}$	1.41 $\times 10^{5}$	1.19 $\times 10^{5}$	1.09 $\times 10^{5}$	1.04 $\times 10^{5}$	1.00 $\times 10^{5}$	9.75 $\times 10^{4}$	9.35 $\times 10^{4}$	8.78 $\times 10^{4}$	8.03 $\times 10^{4}$	8.01 $\times 10^{4}$	6.11 $\times 10^{4}$	4.84 $\times 10^{4}$	3.39 $\times 10^{4}$	1.36 $\times 10^{4}$	4.62 $\times 10^{3}$	1.37 $\times 10^{3}$	3.85 $\times 10^{2}$
12	6.40 $\times 10^{4}$	3.65 $\times 10^{4}$	2.81 $\times 10^{4}$	2.21 $\times 10^{4}$	1.93 $\times 10^{4}$	1.81 $\times 10^{4}$	1.61 $\times 10^{4}$	1.43 $\times 10^{4}$	1.36 $\times 10^{4}$	1.33 $\times 10^{4}$	1.18 $\times 10^{4}$	1.06 $\times 10^{4}$	1.05 $\times 10^{4}$	1.06 $\times 10^{4}$	1.08 $\times 10^{4}$	1.18 $\times 10^{4}$	1.47 $\times 10^{4}$	1.58 $\times 10^{4}$	1.69 $\times 10^{4}$
14	1.90 $\times 10^{5}$	1.96 $\times 10^{5}$	1.53 $\times 10^{5}$	7.90 $\times 10^{4}$	4.70 $\times 10^{4}$	2.51 $\times 10^{4}$	6.53 $\times 10^{3}$	2.77 $\times 10^{3}$	1.08 $\times 10^{3}$	1.01 $\times 10^{3}$	6.53 $\times 10^{2}$	4.91 $\times 10^{2}$	3.34 $\times 10^{2}$	2.37 $\times 10^{2}$	1.66 $\times 10^{2}$	1.40 $\times 10^{2}$	1.44 $\times 10^{2}$	1.57 $\times 10^{2}$	1.67 $\times 10^{2}$
90	2.25 $\times 10^{4}$	2.20 $\times 10^{4}$	2.25 $\times 10^{4}$	2.20 $\times 10^{4}$	2.20 $\times 10^{4}$	2.18 $\times 10^{4}$	2.20 $\times 10^{4}$	2.19 $\times 10^{4}$	2.25 $\times 10^{4}$	2.25 $\times 10^{4}$	2.20 $\times 10^{4}$	2.18 $\times 10^{4}$	2.17 $\times 10^{4}$	2.17 $\times 10^{4}$	2.24 $\times 10^{4}$	2.19 $\times 10^{4}$	1.98 $\times 10^{4}$	1.19 $\times 10^{4}$	4.61 $\times 10^{3}$
106	1.26 $\times 10^{5}$	1.31 $\times 10^{5}$	1.35 $\times 10^{5}$	1.38 $\times 10^{5}$	1.39 $\times 10^{5}$	1.39 $\times 10^{5}$	1.40 $\times 10^{5}$	1.40 $\times 10^{5}$	1.39 $\times 10^{5}$	1.38 $\times 10^{5}$	1.40 $\times 10^{5}$	1.39 $\times 10^{5}$	1.42 $\times 10^{5}$	1.46 $\times 10^{5}$	1.50 $\times 10^{5}$	1.47 $\times 10^{5}$	1.29 $\times 10^{5}$	7.03 $\times 10^{4}$	1.79 $\times 10^{4}$

The depth of the crater formed after sputtering for 40 min was measured with a profilometer and an average sputtering rate of 33nm/min was calculated; this value was used to establish a depth-scale for the P3L09 sputter-profiles. Table 2.5.2 presents the accompanying ion-intensity data as a function of sputtered depth. The oxide-base metal interface was found at a depth of about 1.3 μm in reasonable agreement with the Auger depth-profiling results presented in section 2.3.

Table 2.5.2 clearly shows that the carbon-14 is concentrated in a layer less than 0.2 μm thick close to the surface of the P3L09 sample. Below this depth the carbon-14 concentration is close to its level in the base metal.

In order to obtain a reliable measurement of the carbon-14 concentration in the base metal the P3L09 sample was re-profiled at a high sputtering rate (~300nm/min) to a depth well into the base metal (>10 μm). A flat carbon-14 profile was observed below the oxide/base metal interface with the ^{m}/e-14 ion intensity remaining constant to within ±15%. The resulting surface-to-base metal carbon-14 count rate ratio was estimated to be 1250 ± 190. This agrees well with the ion intensity ratios observed for ^{m} /e-14 in Table 2.5.2 for points close to the surface and the base metal respectively. Similarly the $^{14}C/^{12}C$ ion count ratio in the base metal was found to be $(9 \pm 1) \times 10^{-3}$.

2.6 Total Carbon-14 and Tritium Analysis

High temperature oxidation of the P3L09 sample was carried out as described in section 1.1 of this report. It was found that both the tritium and carbon-14 were released slowly over many hours from the sample at 1100°C. At the end of fifteen hours the sample was completely converted to white zirconium oxide and had released 1.43 μCi of carbon-14 and 7.73 μCi of tritium. Further heating at 1100°C for five hours released less than 0.01 μCi of either carbon-14 or tritium from the sample. In view of the area (0.25 ± 0.01 cm^2) and thickness (0.13 cm) of the specimen it is reasonable to express these values as "surface concentrations":

$$\text{Carbon-14} = 5.7 \pm 0.1\ \mu\text{Ci/cm}^2$$

$$\text{Tritium} = 30.9 \pm 1.1\ \mu\text{Ci/cm}^2$$

As reported in section 2.1, approximately 0.1 μCi/cm^2 of "loose" carbon-14 was removed from the P3L09 sample by ultrasonic agitation showing that more than 95% of the carbon-14 on the pressure tube OD surface is fixed.

3.0 DISCUSSION

The main results emerging from the analysis of the P3L09 pressure tube sample may be summarized as follows:

(i) The OD surface oxide is 1.3 μm to 1.5 μm thick. (A value of 0.8 μm was found for a non-irradiated off-cut)

(ii) Carbon is highly enriched in the outermost surface layer. Below the outer surface the carbon concentration falls rapidly, i.e. within 0.5 μm, to an essentially constant, base metal, level. SIMS data show that the surface carbon is mainly (~80%) carbon-14 but below the surface, at a depth of only 0.1 μm, the carbon-14 concentration decreases to a level below that of carbon-12. (The base metal concentration of carbon-12 is known to be 0.016 wt % /6/)

(iii) Nitrogen is slightly enriched in an outer surface layer ~0.1 μm thick. It is detectable at a maximum concentration of 2.5 at % (~0.3 wt %) (The base metal concentration of nitrogen is known to be 0.006 wt %/6/).

(iv) The P3L09 sample contains 5.7 $\mu Ci/cm^2$ of carbon-14.

In order to interpret these experimental data theoretical estimates of carbon-14 concentrations appropriate to the P3L09 sample are required. Representative calculations are now presented.

3.1 Carbon-14 Concentration Calculations

The required carbon-14 concentration data may be calculated in two ways. Firstly from an Auger depth-profile calibration of SIMS data and secondly from a knowledge of the thermal neutron dose received by, and the nitrogen content of, the P3L09 sample.

1. Carbon-14 Concentration Calculations from a Calibration of SIMS Data

The SIMS ion intensity data for carbon-14 reported in Table 2.5.2 may be put on a concentration basis by using the Auger electron depth-profile data in Table 2.3.1. With the assumption that the sputtering yields of carbon-12 and carbon-14 are equal, the ion count rates for $^{12}C^-$ and $^{14}C^-$ may be added to arrive at a set of total effective ion count rates for carbon. These count rates are plotted as a function of sputtered depth over the range from 0 to 200nm in Fig 3.1. The carbon atomic concentrations from the Auger depth-profiling data in Table 2.3.1 are also plotted on the same graph. The atomic concentration scale interval was chosen to give the best correspondence between the two depth-profiles and thereby calibrate the SIMS count rate data.

To simplify subsequent calculations the carbon-14 distribution in the P3L09 sample may be conveniently divided into two regions of uniform composition, namely a near-surface layer, 50 nm thick, and an inner layer exhibiting the base metal carbon-12 and carbon-14 concentrations.

It may be determined from Fig 3.1 that the average carbon concentration in the outer 50 nm of the P3L09 sample is 10.2 at%. In addition, the data in Table 2.5.2 shows that in this outer layer carbon-14 constitutes 80% of the total carbon. Hence the average surface concentration of carbon-14 is 8.16 at %.

It is readily calculated that a 50 nm layer of ZrO_2 on the 0.25 cm^2 P3L09 sample contains 1.08×10^{17} atoms. Hence, if the number of carbon-14 atoms in the near surface layer is represented by N_s,

$$N_s = \frac{8.16}{100} \times 1.08 \times 10^{17} \text{ atoms/sample}$$

or

$$N_s = 8.81 \times 10^{15} \text{ atoms/sample}$$

The ^{14}C activity is then given by λN_s where λ is the ^{14}C decay constant equal to 3.84×10^{-12}/s. Hence the ^{14}C activity in the surface layer, A_s, is given by,

$$A_s = 8.81 \times 10^{15} \times 3.84 \times 10^{-12} \text{ /s/sample}$$

$$= 3.38 \times 10^{4} \text{ /s/sample}$$

or

$$A_s = 0.91 \ \mu\text{Ci /sample}$$

The carbon-14 in the base metal layer may be calculated as follows:

The P3L09 base metal consists of 0.21g of zirconium containing 0.016 wt % carbon or 1.686×10^{18} atoms of ^{12}C. The $^{14}C/^{12}C$ ion count rate ratio in the base metal was found to be 9×10^{-3}. Hence, if the number of carbon-14 atoms in the base metal is represented by N_B,

$$N_B = 9 \times 10^{-3} \times 1.686 \times 10^{18} \text{/sample}$$

or

$$N_B = 1.52 \times 10^{16} \text{ atoms/sample}$$

The ^{14}C activity in the base metal, A_B, is then

$$A_B = 1.57 \ \mu\text{Ci/sample}$$

The total ^{14}C activity in the P3L09 sample, A_{TOT} is simply $A_s + A_B$, hence,

$$A_{TOT} = 2.48 \ \mu\text{Ci/sample}$$

Since this activity is for a 0.25 cm^2 sample, we may also write,

$$A_{TOT} = 9.92 \ \mu\text{Ci /cm}^2$$

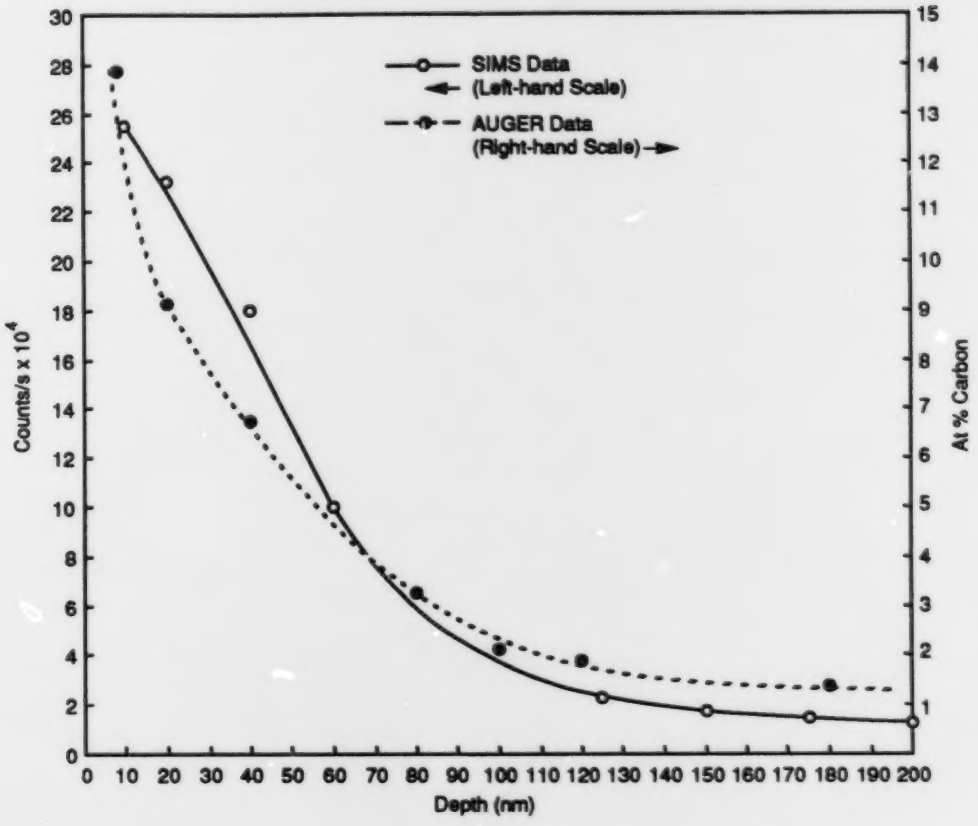

FIGURE 3.1

SIMS/AUGER P3L09 DEPTH - PROFILE INTERCALIBRATION

2. Neutron Activation Calculations

Carbon-14 may be produced by a variety of nuclear reactions e.g. $^{14}N(n,p)\ ^{14}C$, $^{17}O\ (n,\alpha)\ ^{14}C$, $^{13}C\ (n,\gamma)\ ^{14}C$. However, because of the favourable (n,p) reaction cross-section, only the formation from ^{14}N is considered in the present calculations.

In keeping with the approach used above a simple two-layer distribution for the nitrogen in the P3L09 sample is used. Thus, from the Auger depth-profile data in Table 2.3.1, a concentration of 2.5 at% is assumed for a 50nm thick surface layer and the base metal concentration of 0.006 wt % is used for the remainder of the sample.

The number of ^{14}C atoms, N, produced by thermal neutron irradiation of nitrogen is given by,

$$N = N_t\ \sigma\phi t$$

where,

N_t - The number of nitrogen target atoms
σ - The (n,p) reaction cross section - $1.81 \times 10^{-24} cm^2$
ϕ - The thermal neutron flux for P3L09/3/ - $5.7 \times 10^{13}/cm^2/s$
t - The irradiation time - 4240 EFPD - $3.66 \times 10^8 s$

Hence, for activation of the surface layer,

$$N_t = \frac{2.5}{100} \times 1.08 \times 10^{17} \text{ atoms/sample}$$

or

$$N_t = 2.70 \times 10^{15} \text{ atoms/sample}$$

The number of ^{14}C atoms produced in the surface layer, N_s, is given by,

$$N_s = 2.70 \times 10^{15} \times 1.81 \times 10^{-24} \times 5.7 \times 10^{13} \times 3.66 \times 10^8 \text{ atoms /sample}$$

or

$$\underline{N_s = 1.02 \times 10^{14} \text{ atoms/sample}}$$

The ^{14}C activity in the surface layer is then,

$$\underline{A_s = 0.0105\ \mu Ci \text{ /sample}}$$

Similarly for activation of the base metal,

$$\underline{N_t = 5.42 \times 10^{17} \text{ atoms/sample,}}$$

and the number of ^{14}C atoms produced in this layer, N_B, is given by,

$$N_B = 5.42 \times 10^{17} \times 1.81 \times 10^{-24} \times 5.7 \times 10^{13} \times 3.66 \times 10^{8} \text{ atoms/sample}$$

or

$$\underline{N_B = 2.05 \times 10^{16} \text{ atoms/sample}}$$

The ^{14}C activity in the base metal is then,

$$\underline{A_B = 2.13 \ \mu Ci/\text{sample}}$$

The total ^{14}C activity in the P3L09 sample, A_{TOT}, is $A_s + A_B$, hence,

$$\underline{A_{TOT} = 2.14 \ \mu Ci/\text{sample}}$$

or on an area basis,

$$\underline{\underline{A_{TOT} = 8.56 \ \mu Ci/cm^2}}$$

3.2 Comparison of Theory with Experiment

The calculated and measured carbon-14 concentrations found for the irradiated P3L09 sample are summarized in Table 3.2.1. The general agreement between the different total carbon-14 activities reported in Table 3.2.1 is reasonable considering the uncertainties and approximations involved.

Experimentally it was found that carbon-14 is released very slowly from the P3L09 sample heated in air to 1100°C. It is probable that carbon-14 is present as $Zr^{14}C$ in the base metal and this species may not be totally oxidized at 1100°C. It follows that a major portion of the 5.7 $\mu Ci/cm^2$ of carbon-14 liberated from the P3L09 sample originates in the, presumably non-carbidic, surface carbon-14 layer.

The discrepancy between the near-surface carbon-14 activity determined from SIMS data (3.64 $\mu Ci/cm^2$) and the activation calculations (0.04 $\mu Ci/cm^2$) is also significant in this respect. It indicates that the surface carbon-14 is <u>not</u> produced by in-situ activation of nitrogen; the surface enrichment of nitrogen measured by AES and XPS analysis is simply insufficient to account for the high levels of surface carbon-14 observed by SIMS. It is therefore evident that nearly all of the surficial carbon-14 found on the P3L09 sample stems from carbon-14 produced in the nitrogen gas annulus.

Table 3.2.1
Theoretical and Experimental Carbon-14 Activities
in the P3L09 Irradiated Pressure Tube Sample

Method	Near Surface Activity ($\mu Ci/cm^2$)	Base Metal Activity ($\mu Ci/cm^2$)	Total Activity ($\mu Ci/cm^2$)
SIMS Calibration	3.64	6.28	9.9
Activation Calculation	0.04	8.52	8.6
Expt Measurement	-	-	5.7

Calculations show that a total of about 2000 Ci of carbon-14 was formed in the P3 annulus gas system prior to the removal of the L09 pressure tube. The pressure and calandria tubes present a total surface area of approximately 2×10^7 cm^2. Hence, if the carbon-14 was uniformly deposited over these surfaces, a carbon-14 concentration of about 100 $\mu Ci/cm^2$ results. The observed value of 4 to 5 $\mu Ci/cm^2$ therefore constitutes only a small portion of the carbon-14 potentially available for deposition in core. This observation supports the contention made in/2/ and reiterated in/7/ that the heaviest deposition of carbon-14 occurs not on the pressure tube surfaces but out of core on the end-fitting bodies or lattice tubes.

3.3 Carbon-14 Deposition Mechanisms

The carbon-14 distribution found for the P3L09 sample provides some important indications of the carbon-14 deposition mechanism in a gas annulus system. Firstly, very little "loose" carbon-14 was released from the P3L09 sample by ultrasonic agitation; only 0.1 $\mu Ci/cm^2$ or about 2% of the total surface activity. Secondly, SIMS data clearly show that most of the carbon-14 has in fact penetrated at least 10nm below the ZrO_2 surface. These observations are consistent with an ion-implantation mechanism for carbon-14 deposit formation.

Carbon-14 atoms or ions are produced by the ^{14}N $(n,p)^{14}C$ reaction with a recoil energy of 40keV and, as such, have a range of about 0.2 mm in nitrogen /8/. If this range is considered in proportion to the annular gap of 7.6 mm it may be calculated that about 1% of the carbon-14 atoms produced in a gas annulus arrive at the pressure tube OD surface with a kinetic energy >20keV.

At this impact energy ion-implantation is more probable than backscattering by a factor of about five/9/. Consequently it is reasonable to assume that a significant proportion, perhaps up to 2 $\mu Ci/cm^2$, of the near surface carbon-14 is introduced into the pressure tube surfaces by direct ion-implantation of hot carbon-14 species. Range data for keV carbon or nitrogen ions indicate that penetration depths up to 100nm may be attained by this mechanism/8/.

The additional 2-3 $\mu Ci/cm^2$ of carbon-14 needed to account for the observed near-surface concentration of carbon-14 on the P3L09 sample may have been introduced by the indirect process of recoil implantation. Thus thermalized carbon-14 atoms undoubtedly adsorb on the pressure and calandria tube surfaces. It is probable that most of these are transported out of core by the desorption processes discussed in/7/. However a small fraction may also undergo recoil implantation by bombardment with energetic nitrogen ions and become fixed within a few nm of the surface.

It has been pointed out by H. Gaus et. al./10/ that gas phase species in a reactor environment, (nitrogen atoms in the present case), may attain energies up to 250 keV by elastic collisions with fast neutrons. Calculations by the methods outlined in/10/ show that the flux of energetic (ie. > 40 keV) nitrogen atoms to a P3 pressure tube surface is approximately $10^8/cm^2/s$. These ions may become implanted and simultaneously induce recoil implantation of adsorbed carbon-14.

In concluding this section it is worth mentioning that there is evidence that conditions in the P3 gas annulus system have been unusually oxidizing due to substantial air in-leakage/11/. It is probable that carbon-14 fixed into pressure tube oxide scales by the ion-implantation mechanisms proposed above is highly resistant to oxidation. Additional experiments will be required to verify this speculation.

4.0 CONCLUSIONS AND RECOMMENDATIONS

The distribution of carbon-14 in the OD oxide scale on a sample of irradiated pressure tube (L09) from Pickering Unit 3 has been determined by secondary ion mass spectrometry (SIMS) in an ion-microprobe. The SIMS measurements were calibrated by comparison to Auger depth-profile data. It was found that the carbon-14 is located mainly within 50nm of the sample surface at an average concentration of about 8 at %. Below this surface layer the carbon-14 concentration falls rapidly to its base metal level of about 1×10^{-3} at %.

Nitrogen was also found to be enriched in the near-surface region and XRD analysis showed some evidence for a zirconium nitride phase. However, simple calculations show that the in-situ activation of nitrogen cannot account for the observed levels of near-surface carbon-14. It is therefore concluded that carbon-14 was deposited on the P3 sample from the nitrogen gas annulus system probably by an ion-implantation mechanism. In this way up to 5 $\mu Ci/cm^2$ of carbon-14 may have become fixed in the surface oxide in a form resistant to oxidation or dissolution.

It is recommended that additional pressure tube samples should be investigated by the techniques used in the present study to determine the distribution of carbon-14 at different in-core locations. In addition the oxidation kinetics and leachabilty of the carbon-14 should be investigated to provide data useful in developing decontamination and long term waste disposal strategies. As a preliminary step, pressure tube sampling procedures designed to minimize exposure of the carbon-14 to water or other disturbing influences are currently being explored with Hydro and CRNL personnel/12/.

Approved by:

D.J.R. Dodd
Manager
Chemical Research Dept

Prepared by:

F.R.Greening
Chemist
Process Chemistry Section

Reviewed by:

S.H. Hawthorne
Acting Supervising Engineer
Process Chemistry Section

FRG:fc

REFERENCES

1. A. Brennenstuhl. Research Division Report in preparation.

2. F. Greening. The Characterization of Carbon-14 Containing Particulate Material from the Gas Annulus Systems of Pickering NGS 'A' Units 1 and 2 Research Division Report 86-73-K, April 1986.

3. C. Morrison, Design and Development, Private Communication, (June, 1989)

4. JCPDS -Joint Committee on Powder Diffraction Standards. Swarthmore, Penn 19081, U.S.A.

5. H.A. Storms et. al. Evaluation of a Cesium Positive Ion Source for Secondary Ion Mass Spectrometry" Analytical Chemistry 49, 2023 (1977).

6. C. Shulte, Central Production Services, Private Communication, (May, 1989).

7. F. Greening. The Characterization of Carbon-14 Containing Particulate Material from the Gas Annulus Systems of Pickering NGS 'A' Units 1 and 2 - Supplementary Data and Final Conclusions Research Division Report 86-217-K, Oct 1987.

8. L.C. Northcliff et. al. Range and Stopping-Power Tables for Heavy Ions Nuclear Data Tables A7, 233 (1970).

9. J. Bottiger et. al. On the Reflection Coefficient of keV Heavy-Ion Beams from Solid Targets Radiation Effects 11, 69 (1971).

10. H. Guas et. al. Implantation of Environmental Atoms into Solids by Neutron Collisions in Reactors Radiation Effects 18, 79 (1973).

11. F.R. Greening. The Analysis of Samples Associated with the Removal of a Pressure Tube from Pickering NGS 'A' Unit 3 Research Division Report C87-97-K, Nov 1987.

12. C. Frost, Design and Development, Private Communications, (May-June, 1989).

Appendix: P3LO9 Data for Additional Isotopes

While this report deals mainly with the distribution of carbon-14 in the P3LO9 pressure tube OD oxide scale, data for a number of additional isotopes were acquired during analysis of the P3LO9 sample. The experimental results for the isotopes ^{1}H, ^{2}D, ^{3}H, ^{11}B, ^{12}C and ^{13}C are of particular interest and are discussed below.

1. Hydrogen, ^{1}H

Secondary-ion mass spectrometric data for hydrogen are included in Table 2.5.2. Additional depth-profiling measurements were carried out for this isotope to depths up to 10 μm for both the irradiated P3LO9 and non-irradiated P3 off-cut samples.

It was consistently observed that hydrogen decreases quite uniformly, and in parallel with ^{12}C, to a depth of 0.5 μm below the oxide surface. It is concluded that hydrogen is probably present as hydrocarbons in this region.

Below 0.5 μm the hydrogen depth-profiles for the irradiated and non-irradiated samples are different. In the latter case the hydrogen continues to decrease until the base metal is reached. However, in the irradiated sample the hydrogen concentration increases from 0.5 μm to 1.0 μm, ie. the region just above the oxide/base metal interface, as illustrated by the data in Table 2.5.2. Based on calibrations of SIMS data for deuterium (see below) and ignoring isotope effects, a hydrogen concentration of 10^{21} atoms/cm^3 at a depth of 1 μm may be calculated for the P3LO9 sample. By comparison the base metal hydrogen concentration is about 4×10^{19} atoms/cm^3.

The hydrogen distribution in the irradiated P3LO9 sample, after correction for the initial, pre-irradiation, contribution, is typical of an ion-implantation profile. The principal source of energetic protons in a nitrogen gas annulus is the ^{14}N (n,p)^{14}C reaction. It is therefore probable that the hydrogen enrichment observed in the oxide scale of the irradiated P3LO9 sample stems from the 0.58 MeV recoil protons accompanying the formation of ^{14}C. These protons lose an average of about 0.3 MeV in the annulus gas and therefore impact the OD surface of a pressure tube with energies ~0.3 MeV. Protons of this energy have total ranges ~3 μm in ZrO_2. The projected range, which determines the position of the maximum of an implantation profile, is about half of the total range. Thus the observed hydrogen distribution is consistent with the proposed implantation mechanism.

It is also worth noting that if the ^{14}N (n,p) ^{14}C reaction is the source of hydrogen enrichment in pressure tube oxide scales the number of implanted protons should be similar to, but somewhat larger than, the number of implanted ^{14}C atoms. The latter quantity was shown to be 8.8×10^{15} atoms for the P3LO9 sample (see section 3.1). For hydrogen in P3LO9, 10^{21} atoms/cm^3 in a layer 1 μm wide and 0.25 cm^2 in area corresponds to 2.5×10^{16} hydrogen atoms/sample in reasonable agreement with expectations.

2. Deuterium, ^{2}D

Secondary-ion mass spectrometric data for deuterium in the irradiated P3LO9 sample are included in Table 2.5.2. It was found that the deuterium concentration decreases uniformly from the surface to the base metal with only a slight plateau at the oxide/base metal interface. Clearly the deuterium and hydrogen depth-profiles are quite different in the P3LO9 sample indicating that these species enter the oxide by different mechanisms.

Surface Science Western (SSW) have developed methods for the calibration of ion-microprobe data for deuterium in zirconium/1/. Based on these calibrations the deuterium concentration in the P3LO9 sample exhibits a maximum value of 2.0×10^{22} atoms/cm^3 at the oxide surface and falls to 1.5×10^{21} atoms/cm^3 at the oxide/base metal interface. A constant, base metal, deuterium concentration of 2.0×10^{19} atoms/cm^3 is observed below 4 μm.

For the determination of tritium production from deuterium it is useful to consider the deuterium to be divided between a 1 μm layer of ZrO_2 and the Zr base metal. It is then readily calculated that for the P3LO9 sample there are 1.25×10^{17} atoms of deuterium in the oxide and 6.50×10^{17} atoms of deuterium in the base metal.

3. Tritium, ^{3}H

Tritium was determined in the P3LO9 sample only by a bulk radiometric measurement, a time-of-count value of 7.73 μCi being reported in Section 2.5. This converts to 8.57 μCi of tritium at time of shutdown.

Tritium production in CANDU reactors is normally attributed to the $^{2}D\ (n,\gamma)^{3}H$ reaction. Because the deuterium distribution in the P3LO9 sample is known, (see above), it is possible to determine the tritium content of the sample by a straightforward activation calculation provided the rate of deuterium ingress into the P3LO9 pressure tube is known./2/. It will be shown, however, that other sources of tritium are required to account for the observed level of this species in the P3LO9 sample.

For simplicity, and as a worst case, consider deuterium to have entered the pressure tube early in its operating history and remained constant thereafter. Tritium production in the P3LO9 sample by the $^{2}D\ (n,\gamma)^{3}H$ reaction is then given by,

$$A_T = N_t\ \sigma\ \phi\ (1-e^{-\lambda t})$$

where,

A_t is the tritium activity in dis/s at the end of irradiation
N_t is the number of deuterium target atoms = 7.75×10^{17}
σ is the thermal neutron cross-section = 0.52×10^{-27}cm^2
ϕ is the thermal neutron flux for P3LO9 = 5.7×10^{13} n/cm^2/s
t is the irradiation time = 3.66×10^{8}s
λ is the tritium decay constant = 1.79×10^{-9}/s

Hence,

$$A_T = 7.75 \times 10^{17} \times 0.52 \times 10^{-27} \times 5.7 \times 10^{13} \times 0.48 \text{ dis/s}$$

$$= 1.103 \times 10^{4} \text{ dis/s}$$

or, $\underline{A_T = 0.298 \ \mu \text{ Ci/sample}}$

Clearly the theoretical production of tritium from the $^{2}D(n,\gamma)^{3}H$ reaction accounts for only a small fraction (~3.5%) of the tritium experimentally determined in the P3LO9 sample. Consideration of other sources of tritium shows that certain (n,t) reactions are remarkably effective in producing tritium in pressure tubes as illustrated by Table A1. Cross-section data are taken from the literature/3/ and f_T values, the fractions of neutrons above the reaction threshold, are estimated from integration of an assumed $\sinh \sqrt{2E}\, e^{-E}$ neutron spectrum.

Table A1 Theoretical Production of Tritium in the P3LO9 Sample

Nuclear Reaction	N_t (Atoms)	σ (mb)	f_T	Activity (μCi)
$^{2}D(n,\gamma)^{3}H$	7.75×10^{17}	0.52	1	0.298
$^{14}N(n,t)^{12}C$	5.47×10^{17}	20	5.0×10^{-2}	0.404
$^{91}Zr(n,t)^{89}Y$	1.57×10^{20}	0.10	5.6×10^{-3}	0.065
$^{90}Zr(n,t)^{88}Y$	7.20×10^{20}	0.04	2.7×10^{-4}	0.006
$^{93}Nb(n,t)^{91}Zr$	3.50×10^{19}	0.4	1.2×10^{-2}	0.124

Table A1 shows that the $^{14}N(n,t)^{12}C$ reaction is, in fact, more effective than the $^{2}D(n,\gamma)^{3}H$ reaction in producing tritium in the P3LO9 sample.

It has been pointed out that, because of the high cross-section of the $^{3}He(n,p)^{3}H$ reaction, the decay of ^{3}H to ^{3}He actually enhances tritium production in CANDU reactors/4/. If this effect is included in the above calculations the theoretical tritium production in the P3LO9 sample is increased by a factor of about 1.3 for each reaction. However, even after adding all of these enhanced contributions, a total of only about 1.2 μCi or 14% of the experimental value of 8.6 μCi is obtained.

It is concluded that, in analogy to the behaviour of carbon-14, most of the tritium in the P3LO9 sample was not produced by in-situ activation but was introduced from the nitrogen gas annulus. The role of the $^{14}N(n,t)^{12}C$ reaction assumes even greater importance in this case.

4. Boron-11, ^{11}B

As reported in Table 2.5.1, ^{11}B was detected on the surface of the irradiated P3LO9 sample by SIMS. The low levels of boron found in the non-irradiated P3 sample and the virtual absence of ^{10}B in the irradiated sample indicate that the ^{11}B was produced by a neutron induced reaction. The favourable cross-section of the $^{14}N(n,\alpha)^{11}B$ reaction for neutron energies above 3MeV, (~ 300mb), strongly suggests that this is the main production process/3/.

Complete depth-profiles for ^{11}B in the P3LO9 sample were unfortunately not acquired but $^{11}B/^{106}ZrO$ intensity ratio measurements at high and low sputtering rates show the ^{11}B to be highly surface concentrated. Deposition from the gas annulus system, possibly accompanied by recoil implantation, appears to be the main mechanism for the incorporation of ^{11}B into the sample.

5. Stable Carbon Isotopes, ^{12}C and ^{13}C

The SIMS data in Table 2.5.1 reveals some interesting results for the stable carbon isotopes ^{12}C and ^{13}C. The $^{m}/_{e}$ - 13 intensity in the non-irradiated P3 sample is 1.3% of the $^{m}/_{e}$ - 12 intensity; a value of 1.1% is expected for the natural isotopic abundance ratio of ^{13}C to ^{12}C showing that the $^{m}/_{e}$ - 13 peak has only a small contribution from ^{12}CH. Inspection of the equivalent data for the irradiated P3LO9 sample gives a $^{m}/_{e}$ - 13 to $^{m}/_{e}$ - 12 intensity ratio of 2.7% indicating a considerable ^{13}C enrichment after irradiation.

Calculations similar to those presented in section 3.0 of this report show that the cross-section of the $^{12}C\ (n,\gamma)^{13}C$ reaction, (~3.4mb), is too small to produce appreciable ^{13}C enrichment in the surface of the P3LO9 sample. By comparison, the fast neutron reaction $^{16}O\ (n,\alpha)^{13}C$, with a 50mb cross-section for neutron energies above 3MeV, produces ^{13}C in the surface oxide about 100 times faster than $^{12}C(n,\gamma)^{13}C$ and readily accounts for the observed ^{13}C enrichment.

REFERENCES

1. R. Davidson, Surface Science Western, Private Communication, (April - June 1989)

2. C.E. Coleman et. al. Time Scale of Deuterium Ingress by Tritium Dating CRNL Memorandum to B.A. Cheadle, File 2-31-3128-110, (Feb 19, 1988)

3. V. McLane et. al. Neutron Cross-Sections, Vol 2, Neutron Cross Section Curves Brookhaven National Lab. Upton, New York Academic Press (1988)

4. G.F. Thomas et. al. Enhanced Tritium Production for Fusion Reactors Via $^{3}He(n,p)^{3}H$ in the Heavy Water Moderator of a CANDU Reactor Journal of Fusion Energy, 4, 27 (1985)